Available online at www.sciencedirect.com
ScienceDirect
Journal of the European Ceramic Society 31 (2011) 1457–1463
www.elsevier.com/locate/jeurceramsoc

Synthesis and NTC properties of $YCr_{1-x}Mn_xO_3$ ceramics sintered under nitrogen atmosphere

A. Ngueteu Kamlo, J. Bernard, C. Lelievre, D. Houivet *

Université de Caen Basse-Normandie, Laboratoire Universitaire des Sciences Appliquées de Cherbourg (EA 4253), BP 78 – 50130 Cherbourg-Octeville, France

Received 27 October 2010; received in revised form 9 December 2010; accepted 17 December 2010

Abstract

$YCr_{1-x}Mn_xO_3$ ($0 \le x \le 0.8$) negative temperature coefficient (NTC) compositions were synthesized by classical solid state reaction at 1200 °C, and sintered under nitrogen atmosphere at 1500 °C and 1600 °C. XRD patterns analysis has revealed that for $x \le 0.6$, the structure consists of a solid solution of an orthorhombic perovskite $YCrO_3$ phase with Mn substitute for Cr. For $x \ge 0.8$, a second phase with a structure similar to the hexagonal $YMnO_3$ phase appears. SEM images and calculated open porosity have shown that the substitution of Mn for Cr results in a decrease in porosity. Whatever the sintering temperature, the electrical characterizations (between 25 and 900 °C) have shown that the increase in the manganese content involves the decrease in both resistivity and material constant B (parameter which characterizes the thermal sensitivity of material) when $x \le 0.6$. The magnitude order of the resistivity at 25 °C is of 10^4–10^8 Ω cm and activation energies vary from 0.28 to 0.99 eV at low and high temperatures, respectively.

Keywords: A. Powder solid state reaction; C. Electrical properties; D. Perovskites; E. Thermistors; NTC device

1. Introduction

Negative temperature coefficient (NTC) thermistors are the electronic components whose resistance exhibits a significant decrease as temperature increases. Major applications are telecommunications, circuit temperature compensation, temperature measurement, etc.[1] In the literature NTC materials are divided into two groups: low NTC materials, generally work at temperature below 300 °C, consist of transition metal (Cu, Co, Ni, etc.) spinel manganites,[2,3] whereas high NTC materials consist of rare earth (Sm, Tb, Y, ...) perovskite oxides (ABO_3) which can work from ambient to 1000 °C.[4] For NTC applications, the high densification is generally required in order to minimize the ageing phenomenon. $YCrO_3$ perovskite has been considered as a candidate for high temperature thermistors. However, this material is difficult to densify. Tachiwaki et al.[5] have synthesized $YCr_{1-x}Mg_xO_3$ by sol–gel technique using hydrazine and have shown that a 94% relative density is reached at 1800 °C sintering temperature from nano particle size. Even though this chemical method increases the reactivity of the powder (due to its small particles size), it can point out that the raw materials are expensive. In order to study the feasibility of NTC from this type of materials using conventional solid state reaction, Houivet et al.[6,7] have studied the composition aY_2O_3–$bYCr_{0.5}Mn_{0.5}O_3$ ($a+b<1$) and have shown that, at 1600 °C under oxygen atmosphere, densification is improved by increasing the amount of Y_2O_3. Weber et al.[8] have studied the effects of manganese substitution on electrical properties of $Y_{0.9}Ca_{0.1}Cr_{1-x}Mn_xO_3$ ($x=0$, 0.1, 0.2, 0.3), but the sintering temperature and the densification have not been mentioned. The same authors have studied the composition of $Y_{1-x}Ca_xCrO_3$[9] synthesized by glycine–nitrate process and shown that calcium improves relative density. It can underline that the substitution of Y^{3+} for Ca^{2+} influences the diffusion phenomenon and electrical conductivity. In fact, the replacement of a trivalent ion by a divalent ion is electrically compensated by the formation of tetravalent chromium at high oxygen pressure.[8,10] Thus, the resistivity significantly drops after replacement and their application is only limited at low temperature. In general, NTC materials are sintered under air whereas the change of

* Corresponding author. Tel.: +33 233014233; fax: +33 2 33 01 41 35.
E-mail address: david.houivet@unicaen.fr (D. Houivet).

0955-2219/$ – see front matter © 2011 Elsevier Ltd. All rights reserved.
doi:10.1016/j.jeurceramsoc.2010.12.025

atmosphere can improve densification. The present paper deals with the effect of the manganese substitution on densification and NTC properties of $YCr_{1-x}Mn_xO_3$ sintered under nitrogen atmosphere. It is important to note that the substitution concerns both Mn and Cr which can take the same valency.

2. Experiments

The compositions were prepared by weighing in appropriate proportions of reagent grade oxides: Y_2O_3 (Jonhson Matthey, 99.99%), Cr_2O_3 (Riedel-dehäen, 99%), Mn_2O_3 (Aldrich, 99%). The weighed raw materials were mixed and ground for 2 h using 0.8–1 mm yttria stabilised zircon balls in a laboratory attrition mill. The slurry solid load is 40 wt% and the dispersion liquid is an aqueous ammoniac solution at pH = 11, in order to obtain a good repulsion between particles and a low slurry viscosity. The powders were dried and then calcined at 1200 °C in a Pyrox furnace under air. Calcined powders were mortar disagglomerated. Cylindrical pellets (5 mm diameter, 2.5–3.5 mm height) were obtained by uniaxial pressing at 2 T/cm^2 for sintering. Pellets were sintered at two different temperatures of 1500 °C and 1600 °C under nitrogen flow for 5 h.

Specific surface area of powders was measured by BET method using a Tristar II Micromeritics after drying at 300 °C under vacuum. Thermodilatometric measurements were performed up to 1600 °C with Setaram TMA 92 under nitrogen. The density of sintered pellets was measured by a helium pycnometer accupyc 1330. Calcined powders at 1200 °C and sintered samples were characterized by X-ray diffraction (Siemens D5005, Cu Kα radiation). The microstructure of sintered samples was observed by the Scanning Electron Microscope (SEM, Hitachi S3460) in combination with energy dispersive spectroscopy (EDS, ThermoNoran). For electrical characterization, the two opposite faces of pellets were coated by platinum paste and annealed at 1200 °C. Electrical bulk resistances were measured from ambient to 900 °C, using Enertec 7150 digital multimeters. The electrodes and wires are made in platinum in order to avoid generating a thermocouple. The first step consists in measuring only the resistance of wire and electrode versus temperature without sample. The second step consists in measuring the total resistance (wire + electrode + sample) versus temperature. The third step consists in subtracting to the total resistance, the resistance of wires and electrodes. The energetic material constant B, proportional to the sensitivity of thermistor, is obtained using the Arrhenius-type equation $\rho = \rho_o \exp(B/T)$ where ρ, is the resistivity of the sample at a given temperature, ρ_o the resistivity of the sample at room temperature (25 °C) and T the absolute temperature. From B constant, activation can be expressed by the relation $B = Ea/k$, where Ea is the activation energy and k the Boltzmann constant.

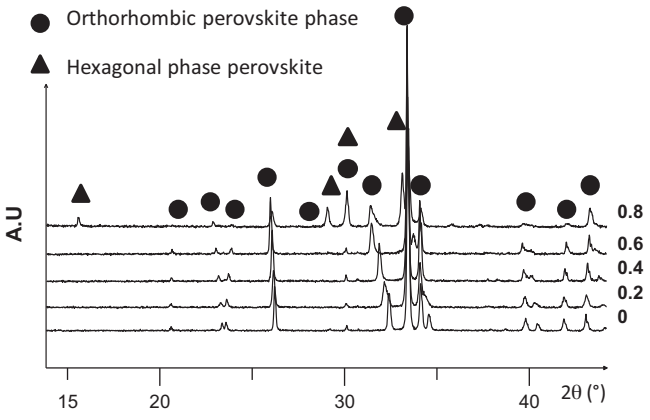

Fig. 1. XRD patterns of different calcined.

Table 1
Cell parameters, cell volumes, and orthorhombicity parameters of different calcined powders.

x	a (Å)	b (Å)	c (Å)	V (Å^3)	b/a
0	5.520	7.539	5.259	218.84	1.366
0.2	5.561	7.505	5.254	219.29	1.350
0.4	5.608	7.495	5.264	221.25	1.336
0.6	5.680	7.455	5.261	222.79	1.313
0.8	5.688	7.453	5.206	220.70	1.310

3. Results and discussions

3.1. Calcined powders characterizations and sintering behaviour

The BET specific area values of different compositions after calcination range from 1 to 1.6 m^2/g. Fig. 1 shows the X-ray diffraction patterns of $YCr_{1-x}Mn_xO_3$ ($0 \le x \le 0.8$) calcined powders at 1200 °C. The analysis of these diffractograms has revealed that, for x under 0.8, the presence of a single phase isomorphic to the orthorhombic perovskite $YCrO_3$ ((JCPDF 00-034-0365), space group *Pnma* (62)) with a shift of the position of certain peaks function of the composition. The substitution of manganese for chromium in $YCrO_3$ affects the lattice parameters as can be seen in Table 1. The incorporation of Mn leads to an increase in "a" and a decrease in "b" lattice parameters. Apart from $x = 0.8$, "c" parameter remains almost unchanged. This variation can be related to the ionic radii of Mn^{3+} and Cr^{3+} (for octahedral coordination, $R_{Mn^{3+}} = 0.65$ Å, $R_{Cr^{3+}} = 0.62$ Å). Therefore, the Mn substitution for Cr implies a small change of the octahedral distortion and induces an increase in cell volume which is in agreement with the difference of ionic radii (Table 1 and Fig. 2). A similar behaviour has been observed in different compositions such as $La(Cr_{1-y}Mn_y)O_3$,[11] $YFe_{1-x}Cr_xO_3$,[12] $Y(Cr_{1-x}Mg_x)O_3$,[13] $Y(Co,Mn)O_3$.[14] In Fig. 2, it can be see that, for $x \le 0.6$, this increase in the cell volume with x (Mn substitution) seems to follow a linear law. Kostikova and Kostikov[15] think that this law can be used as a valuable tool for validating the presence of a limited solid solution. Thus, it may be suspected that an orthorhombic perovskite $YCr_xMn_{1-x}O_3$ would be a limited solid solution for $x \le 0.6$.

For x equals to 0.8, the indexation of the structures clearly indicates two phases. The main phase is closed to the hexagonal structure $YMnO_3$ (JCPDF 01-070-4962, space group *P*63*cm*) associated with a second phase "$YCrO_3$" type. The appearance of "$YMnO_3$" for $x = 0.8$ would indicate that there is a limit of

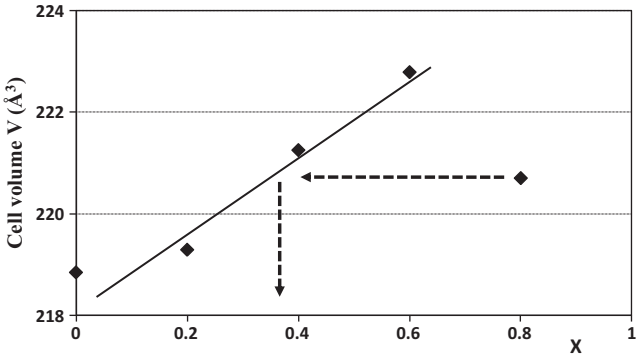

Fig. 2. Cell volume versus manganese content of the orthorhombic perovskite phase for calcined powders.

solubility of Mn in the orthorhombic structure "$YCrO_3$". This limit is between $x = 0.6$ and $x = 0.8$ of manganese content. For these compositions, Ismailzade et al.[16] have reported the value of 0.55 of manganese content as a limit of solubility when the materials are synthesized at 1400 °C in air. The difference could be linked to the synthesis temperature and the nature of the mixing process. At first sight, the decrease in the orthorhombic "$YCrO_3$" cell volume for $x = 0.8$ can be surprising. In fact, it can be related to the limit of solubility. Only a fraction of the $x = 0.8$ manganese content contributes to the orthorhombic structure. From Fig. 2, for the $x = 0.8$, the projection of the cell volume on the straight line tends to show that the manganese content in the perovskite phase is between 0.3 and 0.4. The remainder manganese belongs to the hexagonal phase. So for $x = 0.8$ the two phases are an orthorhombic perovskite $YCr_{1-y}Mn_yO_3$ phase with $0.3 < y < 0.4$ and a hexagonal $YMn_{1-z}Cr_zO_3$ phase.

Fig. 3 shows the thermodilatometric measurements up to 1600 °C under nitrogen atmosphere for different compositions. This experiment was performed in order to optimise the sintering temperature. As can be seen on the graph, the starting shrinkage temperature slightly decreases with increasing the Mn substitution for Cr. For $x = 0$, it is clear that there is no shrinkage at 1600 °C. This means that the first step of densification does not take place. This is the reason why, this composition ($x = 0$) was not sinter in the present work. For x higher than 0.2, the curves tend to show that the sintering is roughly completed. Although final shrinkage can also be related to the relative density degree,

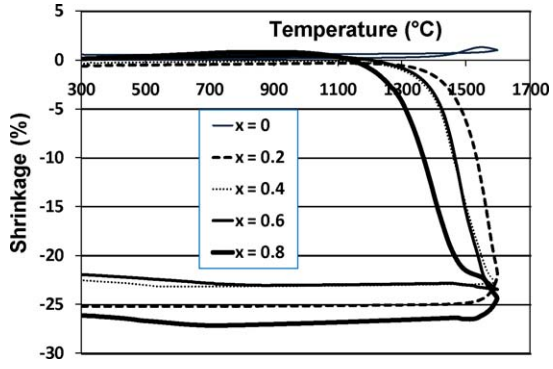

Fig. 3. Dilatometric curves versus x – manganese fraction.

in this case, the comparison has no sense because the green densities are not necessarily the same. It is due to the different compositions. Thus, in order to study the effect of manganese substitution in the same temperature conditions, two sintering temperatures were fixed at 1500 °C and 1600 °C. We are aware that densities can be different for compositions sintered at a same temperature, but it is difficult to work at constant density with a appropriate temperature to each composition.

3.2. Structure and microstructure characterizations of sintered samples at 1500 and 1600 °C

After sintering at 1500 °C and 1600 °C, XRD patterns of sintered pellets are very similar to calcined powders, so XRD patterns are not shown here. The only difference is for the composition $x = 0.8$ sintered at 1600 °C, a single hexagonal phase structure-type $YMnO_3$ is observed. For $x = 0.8$, the disappearance of the orthorhombic perovskite structure tends to confirm that the limit of solubility of Cr in the hexagonal structure $YMnO_3$ increase with temperature.

The SEM micrographs of polished and sintered samples are reported in Fig. 4. For x ranging from 0.2 to 0.6, the microstructure of sintered samples at 1500 °C is very porous whereas for $x = 0.8$ it is well densified. This is in accordance with the results of open porosity (for instance, porosity $\geq 33\%$ for $x \leq 0.4$) obtained via pycnometer measurements and plotted in Fig. 5. However, the porosity significantly decreases when samples are sintered at 1600 °C. For the same composition, Fig. 5 has clearly shown an improvement of densification as sintering temperature increases. This is due to the fact that the diffusion mechanism is promoted by temperature. Porosity and SEM images indicate that the higher the substitution x is, the lower the porosity is. In taking into account the cell volume and orthorhombicity parameters obtained from XRD patterns, it can be said that the distortion of octahedral coordination of Cr/Mn in $YCr_{1-x}Mn_xO_3$ increases as the manganese content increases. This distortion could improve the rate of diffusion and then the densification phenomenon. Open porosity highly depends on the nature of phase. Whatever the sintering temperature, orthorhombic structure phases ($x = 0.2, 0.4, 0.6$), are more porous than the hexagonal structure ($x = 0.8$).

At 1500 °C, for $x \leq 0.6$, SEM images exhibit homogeneous microstructures that could correspond to the single perovskite structure observed by the XRD patterns. Nevertheless, for $x = 0.8$, SEM images show a biphasic microstructure and a grain growth. EDS analysis revealed that the grey phase is Y-rich and Mn-rich (about 55% Y, 42% Mn, 3% Cr) whereas the black phase is Mn-rich (16% Y, 81%Mn, 3% Cr).

At 1600 °C, each composition has revealed a uniform microstructure which can be attributed to a single orthorhombic perovskite phase for $x \leq 0.6$ and hexagonal phase for $x = 0.8$. It is noticeable that a rise in manganese fraction engenders an important grain growth. For instance, the grain size is about 4–8 μm for $x = 0.4$, 15–30 μm for $x = 0.6$ and can reach up to 50 μm for $x = 0.8$. One has to emphasize the sintering at 1600 °C involves the disappearance of the Mn-rich phase observed for the sintered samples at 1500 °C. It leads us to think that not only is this phase

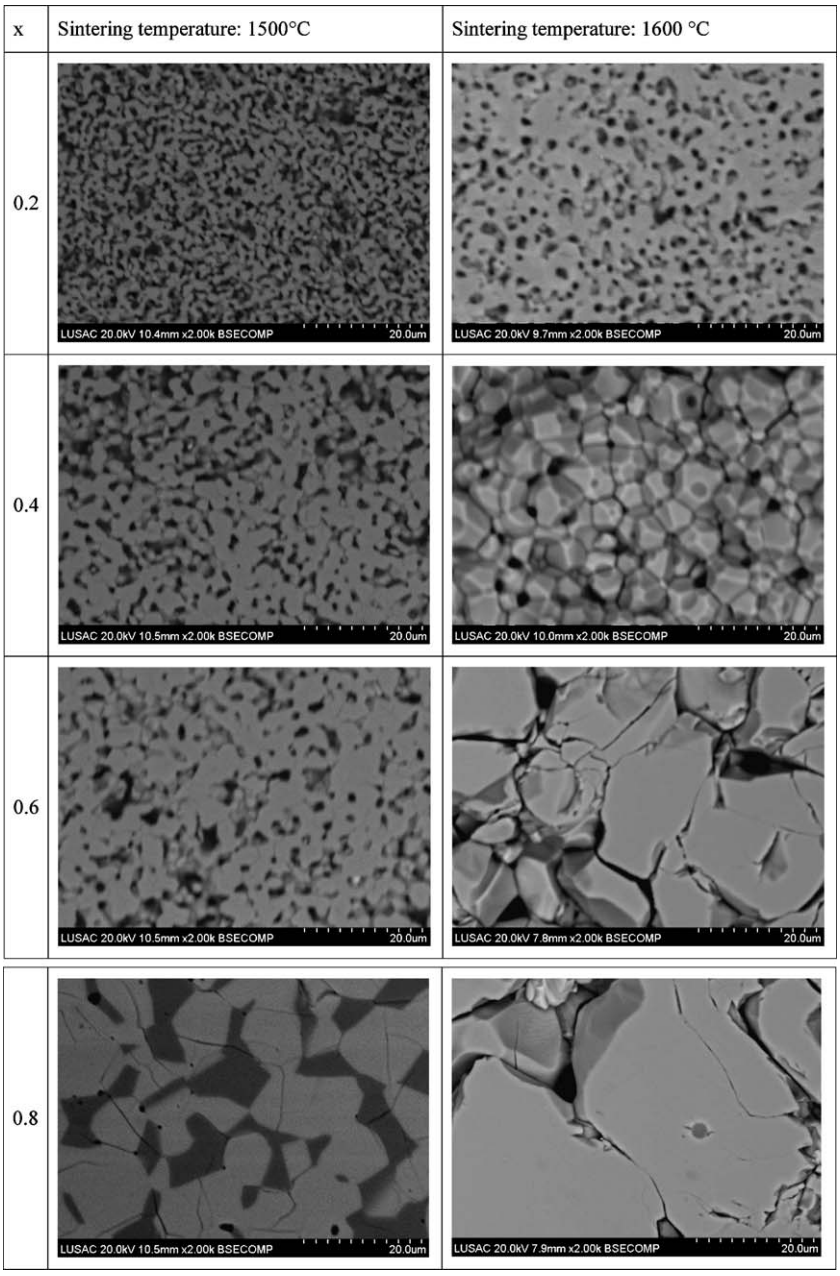

Fig. 4. SEM micrographs of the sintered samples regions at different dwell times at 1500 and 1600 °C.

thermally unstable, but the limit of solubility of manganese is also temperature-dependant.

3.3. NTC electrical properties

Electrical properties were investigated from 25 to 900 °C. The resistivity is calculated from the measured resistance. From these data, the energetic constant material (B) and the activation energy are calculated. As can be seen in Fig. 6a and b, which represent the ln of the resistivity ρ versus $1/T$, the results clearly reveal that the resistivity is manganese content-dependent and the electrical behaviour is NTC (negative temperature coefficient, i.e. the resistivity decreases when T increases). Whatever the sintering temperature, the bulk resistivity of $YCr_{1-x}Mn_xO_3$

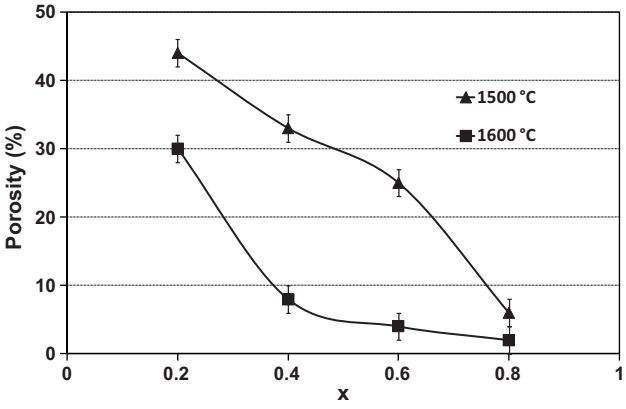

Fig. 5. Porosity of $YCr_{1-x}Mn_xO_3$ sintered at 1500 and 1600 °C.

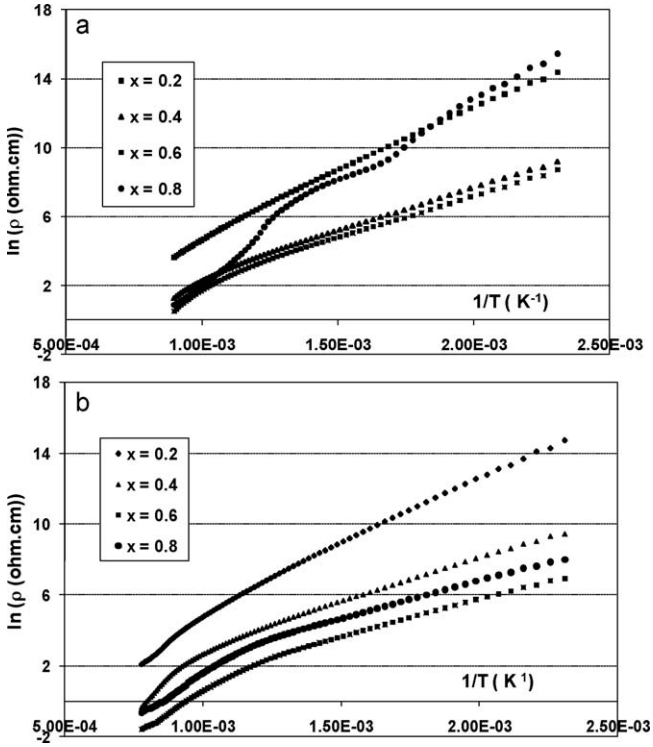

Fig. 6. Ln(resistivity ρ) as a function of $1/T$ $YCr_{1-x}Mn_xO_3$: sintered samples at (a) 1500 °C and (b) 1600 °C.

decreases when the manganese content increases from $x = 0.2$ to 0.6. However, for the composition $x = 0.8$, there is an unexpected trend. This abnormal evolution could be linked to the difference nature of phase structure. In fact, from $x \leq 0.6$, the structure is perovskite-type whereas it is hexagonal-type for $x = 0.8$. The curve of the sintered sample ($x = 0.8$) at 1500 °C is very irregular (Fig. 6a). Irregular NTC characteristics for this composition could be attributed to the Mn-rich second phase as we have seen on SEM images for this sample. This assumption is supported by the fact that, for the same composition sintered at 1600 °C but with only a single hexagonal phase, the electrical resistivity behaviour versus reciprocal temperature is totally different. Apart from $x = 0.8$ sintered at 1500 °C, the resistivity of the other samples have revealed a change of slope at about 600 °C ($1/T = 1.14 \times 10^{-3}$ K^{-1}). Above and below this temperature, resistivity fits an Arrhenius law. Generally, the straight line observed by plotting $\ln \rho$ or $\ln(\sigma/T)$ versus $1/T$ is characteristic of small polaron hopping transport phenomenon which is often in chromium based perovskites.[17,18] Thus, we assume that the mechanism in the samples could be due to the small polaron mechanism. This mechanism can be described by the relation: $\sigma = 1/\rho = (C/T)\exp(-Ea/kT)$,[19–22] where σ is the electrical conductivity, ρ the electrical resistivity, C the charge carrier concentration, T the absolute temperature, Ea the activation energy and k Boltzmann's constant. As the resistivity decreases as manganese content increases, it may be assumed that manganese could promote the rise in charge carriers, C, and then the hopping mechanism. Verwey et al.[23] have shown that, in the case of manganite oxides in which the octahedral sites contain two ions of the same element, with different oxidation numbers, the electrical conduction taking place by polarons jumps between neighbouring ions. Knowing that, the B-site of $YCr_{1-x}Mn_xO_3$ perovskite phase contains both manganese and chromium elements, which have different valency states, one can assume the possibility of electron jumps between different oxidation states of chromium ions on the one hand and different oxidation states of manganese on the other hand. The study of grade of reduction of cations will be later performed in another paper. For the orthorhombic phase structure ($x = 0.2$, 0.4, 0.6), the increase in C with manganese content increasing engenders the rise in electrical conductivity, that is to say the decrease of electrical resistivity as plotted in Fig. 6a and b. For the hexagonal phase ($x = 0.8$ sintered at 1600 °C), the resistivity is inferior to the one observed for orthorhombic phase ($x = 0.6$). This could be due to the fact that, in hexagonal phase, manganese does not have octahedral oxygen surroundings like orthorhombic phase. In this case, the hopping distance is also different. As mentioned above, the slope of the $\ln(\rho)$ versus $(1/T)$, which represents the B constant, changes around 600 °C. That is the reason why B constants (Tables 2 and 3) at low (25–150 °C) and high temperatures (700–800 °C) are cal-

Table 2
Electrical properties of NTC sintered samples as function of manganese content at 1500 °C.

x	$\rho_{25\,°C}$ (Ω cm)	$B_{25–100\,°C}$ (K)	$B_{700–800\,°C}$ (K)	$Ea_{25–100\,°C}$ (eV)	$Ea_{700–800\,°C}$ (eV)
0.2	1.7×10^8	5062	9521	0.43	0.82
0.4	3.1×10^5	3984	8481	0.34	0.73
0.6	2.3×10^5	3896	7829	0.34	0.67
0.8	1.1×10^8	5356	11,520	0.46	0.99

Table 3
Electrical properties of NTC sintered samples as function of manganese content at 1600 °C.

x	$\rho_{25\,°C}$ (Ω cm)	$B_{25–100\,°C}$ (K)	$B_{700–800\,°C}$ (K)	$Ea_{25–100\,°C}$ (eV)	$Ea_{700–800\,°C}$ (eV)
0.2	1.3×10^8	5000	11,324	0.43	0.98
0.4	3.5×10^5	3774	11,000	0.32	0.95
0.6	3.9×10^4	3266	10,714	0.28	0.93
0.8	5.6×10^4	3318	11,107	0.29	0.96

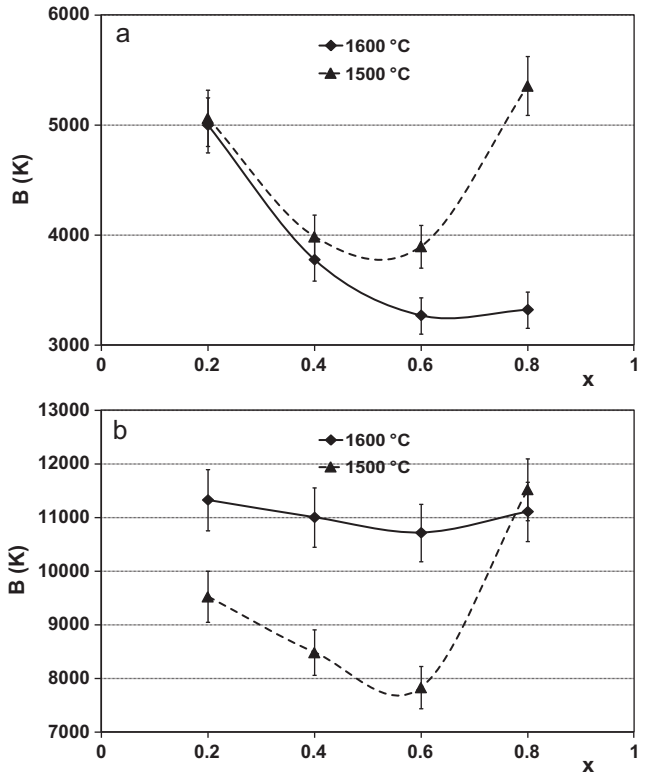

Fig. 7. Energetic constant material as function of manganese constant: (a) at low temperature (25–150 °C) and (b) at high temperature (700–800 °C).

culated and plotted in Fig. 7a and b. For the same structure and for a given sintering temperature, B decreases with manganese content. At low temperature B-values are ranging from 5062 K to 3266 K and correspond to 0.43 eV and 0.28 eV as activation energy, respectively, whereas at high temperature, B-values are ranging from 7829 K to 11,520 K with 0.67 eV and 0.99 eV, respectively. The sharp increase in Ea at high temperature tends to show that there is either a new or an additional mechanism which controls the conduction mechanism at high temperature.

4. Conclusions

For NTC applications, different compositions of $YCr_{1-x}Mn_xO_3$ were prepared by conventional solid state reaction at 1200 °C and sintered under nitrogen atmosphere at 1500 and 1600 °C. XRD patterns have revealed that the phase of calcined powders and sintered pellets depends on the content of manganese substitution. For $x \leq 0.6$, which corresponds to the limit of solubility, the structure consists of an $YCrO_3$ orthorhombic perovskite solid solution with Cr substitute for Mn. Beyond $x \geq 0.8$, the new phases appears. SEM micrographs and calculated open porosity have shown that, in general, the more the manganese content, the lower the porosity is. The negative temperature coefficient parameters, the resistivity (ρ) and material constant (B), highly depend on the manganese content. In the studied compositions, the magnitude order resistivity at 25 °C is ranging from 10^4 to 10^8 Ω cm and activation energy from 0.28 to 0.99 eV. These compositions could be used as potential candidates for NTC thermistors in a large range of temperature from ambient to 900 °C.

Acknowledgments

We thank the regional council of Basse-Normandie, the French Government (CPER GR^{2}TC project) and The European Community (FEDER funds) for their financial supports.

References

1. Buchman RC. *Ceramic materials for electronics*. New York: Marcel Dekker; 1986.
2. Rousset A, Legros R. *Journal of European Ceramic Society* 1994;**13**:185–95.
3. Battault T. Céramiques semi-conductrices à base de manganites, de fer, nickel et cobalt. Application aux thermistances à coefficient de température négatif (C.T.N), Thesis of University Paul Sabatier, Toulouse, 1995.
4. Sache BH. *Semiconducting temperature sensors and their applications*. New York: John Wiley; 1975.
5. Tachiwaki T, Kunifusa Y, Yoshinaka M, Hirota K, Yamaguchi O. Formation, densification, and electrical conductivity of air-sinterable $YCr_{1-x}Mg_xO_3$ prepared by hydrazine merthod. *International Journal of Inorganic Materials* 2001;**3**:107–11.
6. Houivet D, Bernard J, Haussonne JM. High temperature NTC ceramics resistors (ambient −1000 °C). *Journal of European Ceramic Society* 2004;**24**:1237–41.
7. Haussonne JM. *Céramiques pour l'électronique et l'électrotechnique*. Lausanne: Presses Polytechniques et Universitaires Romandes; 2002.
8. Weber WJ, Griffin CW, Bates JL. The effets of cation substitution on electrical and thermal transport of properties of $YCrO_3$ and $LaCrO_3$. *Journal of American Ceramic Society* 1987;**70**:265–70.
9. Bates JL, Chick LA, Weber WJ. Synthesis, air sintering and properties of lanthnum and yttrium chromites and manganites. *Solid State Ionics* 1992;**52**:235–42.
10. Anderson HU. Development of improved cathodes for solid oxide fuel cells, University of missouri, Contract No.: DE-FG21-89MC26015, 1992:1–28.
11. Tseggai M, Tellgren P, Rundlöf H, Andrè G, Bourèe F. Synthesis, nuclear, and magnetic properties of $La(Cr_{1-y}Mn_y)O_3$ ($y = 0$, 0.1, 0.2 and 0.3). *Journal of Alloys and Compounds* 2008;**437**:532–40.
12. Dahmani A, Taibi M, Aride J, Belayachi A, Nogues M. Magnetic properties of the perovskite compound $YFe_{1-x}Cr_xO_3$ ($0.5 \leq x \leq 1$). *Materials Chemistry and Physics* 2002;**77**:912–7.
13. Tachiwaki T, Kunifusa Y, Yoshinaka M, Hirota K, Yamaguchi O. Formation, densification and electrical conductivity of air-sinterable $Y(Cr_{1-x}Mg_x)O_3$ prepared by the hydrazine method. *Materials Science and Engineering B* 2001;**86**:255–9.
14. Gutiérrez D, Peña O, Ghanimi K, Durán P, Moure C. Electrical and magnetic features in the perovskite-type system $Y(Co,Mn)O_3$. *Journals of Physics and Chemistry of Solids* 2002;**63**:1975–82.
15. Kostikova GP, Kostikov YP. Application of Vegard law to the description of solid-solutions. *Inorganic Materials* 1993;**29**:1005–6.
16. Ismailzade I, Smolenskii G, Nesterenko V, Agaev F. X-ray electric investigations of the systems $Y(Mn_{1-x}B_x)O_3$ ($B = Fe^{3+}$, Cr^{3+}, Al^{3+}). *Physica Status Soidil (a)* 1971;**5**:83–9.
17. Basal KP, Kumari S, Das BK, Jain GC. On some properties of strontium-doped lanthanum chromites. *Journal of Material Sciences* 1983;**18**(7):2095–100.
18. Gaur K, Verma SC, Lal HB. Defects and electrical conduction in mixed lanthanum transition metal oxides. *Journal of Material Sciences* 1988;**23**(7):1725–8.

19. Karim DP, Cox DE. Structural studies of the (La,Sr)CrO_3 system. *Materials Research Bulletin* 1977;**12**:463–72.
20. Austin IG, Mott NF. Polarons in crystalline and non crystalline materials. *Advanced Physical* 1969;**18**:41–102.
21. Goodenough JB. Metallic oxides, p. 145–399, In: Reiss H. editor. Solid State Chemistry, vol. 5. Pergamon Press, New York; 1971, in progress.
22. Heikes DR. Studies of small polaron motion, part 4. Adiabatic theory of hall effect. *Annals of Physics, New York* 1969;**53**: 439–520.
23. Verwey EJW, Haayman PW, Romeyn FC. Semiconductors with large negative temperature coefficient. *Philips Technical Review* 1947;**9**: 239–48.